Canadian Journal of
Fisheries and
Aquatic Sciences

Article

No free lunch: estimating the biomass and ex-vessel value of target catch lost to depredation by odontocetes in the Hawai‘i longline tuna fishery

Joseph E. Fader[a], **Jamie A. Marchetti**[b], **Robert S. Schick**[c], **and Andrew J. Read**[a]

[a]Duke Marine Lab, Division of Marine Science and Conservation, Nicholas School of the Environment, 135 Duke Marine Lab Road, Beaufort, NC 28516, USA; [b]Pacific Islands Regional Office, National Marine Fisheries Service, NOAA, Honolulu, HI, USA; [c]Nicholas School of the Environment, Duke University, Durham, NC, USA

Corresponding author: **Joseph E. Fader** (email: joefader@gmail.com)

Abstract

Depredation by marine predators causes economic losses and impacts depredating species and fish stocks. To understand these impacts, it is important to accurately estimate catch losses from depredation. Pelagic longline fisheries are susceptible to depredation, and depredation is difficult to quantify, because gear is suspended in the water column away from the vessel for extended periods. In the present study, we used fisheries data and a novel modeling approach to estimate catch removal by odontocetes in the Hawai‘i deep-set longline fishery. We estimated annual biomass and economic value lost to depredation of three of the most commonly landed species as approximately 100 t and 1 million USD, respectively, during 2012–2018. The median cost on sets when depredation occurred was $600 USD, with the worst 10% of sets experiencing losses exceeding $2300 USD. We also identified broad-scale spatiotemporal patterns and hotspots of depredation across the range of the fishery. Our findings quantify the ecological and economic implications of this interaction, and our methods can be applied in similar fisheries elsewhere to assess the impacts of depredation.

Key words: depredation, false killer whale, fisheries interactions, odontocete, pelagic longline fishery

1. Introduction

The expansion of human exploitation of marine living resources during the past century has created and exacerbated conflicts between fisheries and top predators (Lewison et al. 2004, 2014; Guerra 2019). Some interactions are indirect, such as competition with predators for shared resources or other trophic effects arising from exploitation of target species (Branch et al. 2010; Morissette et al. 2010). Others are more direct, such as entanglement and bycatch. Predators are also known to feed directly on bait or fish secured on fishing gear, an interaction known as depredation (Gilman et al. 2007, 2008; Tixier et al. 2020*b*). A wide range of marine predators are known to engage in depredation with a diverse array of fishing gear (Tixier et al. 2020*b*). The impacts of depredation extend to fishermen, predators, and ecosystem structure and function (Gilman et al. 2007, 2008; Hamer et al. 2012; Mitchell et al. 2018).

Depredation can lead to substantial socioeconomic costs for affected fisheries (Peterson et al. 2014; Tixier et al. 2020*a*). These include direct costs from damage to gear and loss of bait or catch, and indirect costs caused by increasing fishing effort to make up for lost catch or fuel costs from moving to avoid areas of known depredation (Tixier et al. 2020*b*). Depredating species are also affected in multiple ways. Feeding on restrained catch may have population consequences such as changes in habitat use (Blasi et al. 2015) or reduced energetic costs of foraging and access to new foraging opportunities (Esteban et al. 2016). Depredation also increases the risk of injury or mortality due to hooking or entanglement in fishing gear (Forney et al. 2011) and retaliatory responses from fishermen (Poncelet et al. 2010; Guinet et al. 2015). Finally, depredation can lead to higher exploitation rates of fish stocks and bias in stock assessments, as depredated catch is not typically included in estimates of fishing mortality (Peterson et al. 2013; Esteban et al. 2016; Peterson and Hanselman 2017; Hanselman et al. 2018). Thus, it is important to obtain accurate estimates of catch losses accruing from depredation to understand these diverse ecological and socioeconomic impacts.

Longline fisheries are particularly susceptible to depredation as bait and catch are typically suspended in the water column without any protection or barrier from predators (Gilman et al. 2007, 2008; Tixier et al. 2020*b*). Depredation has been reported in longline fisheries by cetaceans, sharks, squid, and seabirds (Tixier et al. 2020*b*). Depredation by odontocete cetaceans is particularly common and problematic for fishermen. Some odontocete species are skilled in locating fishing gear, sequentially removing fish as gear is hauled

or traveling along lengths of gear to remove bait or catch (Towers et al. 2019; Anderson et al. 2020). These behaviors can lead to substantial economic costs to affected fishermen (Peterson et al. 2014; Tixier et al. 2020*a*).

In Hawai'i, two pelagic longline fisheries experience odontocete depredation and bycatch. The deep-set fishery targets bigeye tuna (*Thunnus obesus*, Scombridae) and operates year-round on the north and south of the Hawaiian Islands, both inside and outside of the U.S. Exclusive Economic Zone (EEZ) (Supplementary Material, Fig. S1). A smaller, shallow-set fishery operates mainly north of the Hawaiian Islands targeting swordfish (*Xiphias gladius*, Xiphiidae). Odontocete depredation and bycatch is more common in the deep-set fishery (Forney et al. 2011), where false killer whales (*Pseudorca crassidens*, Delphinidae) depredate bait and catch, and are the most common species of cetacean taken as bycatch (Thode et al. 2016; Bayless et al. 2017). Other odontocete species such as short-finned pilot whales (*Globicephala macrorhynchus*, Delphinidae) and Risso's dolphins (*Grampus griseus*, Delphinidae) are also occasionally recorded as bycatch, likely driven by depredation as well (Forney and Kobayashi 2007; Forney et al. 2011; Fader et al. 2021). Unsustainable levels of false killer whale bycatch have led to regulatory actions by the National Marine Fisheries Service (NMFS), following recommendations from the False Killer Whale Take Reduction Team (FKWTRT), a multistakeholder group charged with reducing mortality and serious injury of false killer whales below levels stipulated by the U.S. Marine Mammal Protection Act (Federal Register 2010). The FKWTRT has recommended gear changes, handling requirements, and spatiotemporal closures that are triggered when false killer whale bycatch exceeds certain levels. These restrictions impart additional costs to the fishery beyond losses due to depredation itself.

There are a few video records of false killer whales depredating bait and acoustic recordings of false killer whales near depredated gear (Thode et al. 2016; Bayless et al. 2017). However, in general, depredation by odontocetes is rarely observed directly in the deep-set fishery. Instead, depredation of catch is typically inferred by characteristic damage to individual fish retrieved during the haul (Forney et al. 2011; Fader et al. 2021). Studies to date have focused on characterizing depredation patterns to inform potential mitigation solutions (Forney et al. 2011; Fader et al. 2021). Despite the high value of the target species in this fishery, to date there have been no rigorous, quantitative assessments of the economic impact that depredation has on the fishery or the potential effects of these losses on target stocks. TEC Inc. (2009) reported estimates of fish biomass lost and economic implications due to odontocete depredation, but these estimates were based on estimates provided by fishermen of the proportion of total catch lost per depredated set. In this paper, we use a novel modeling approach incorporating observer-collected and logbook fishery data to estimate removals of commercially important catch by odontocetes in the Hawai'i deep-set longline fishery. We first predict the species and size of individual depredated fish, and we then scale these estimates to assess fishery-wide removals and assess broad-scale spatial and temporal patterns of depredation across the range of the fishery.

2. Methods

2.1. Data sources and data preparation

2.1.1. Study area and fishery-dependent data sources

Hawai'i deep-set gear consists of a single monofilament mainline (3.2–4.0 mm diameter), suspended in the water column by a series of floats (Supplementary Material, Fig. S2). Between each float, individual, monofilament branch lines are regularly spaced, each terminating with a single bait fish (saury or sardine) attached to a circle hook (Boggs and Ito 1993). The target depth for bigeye tuna is around 400 m and typical deployment of fishing gear ranges from 1000 to 3000 hooks over ~45–80 km of mainline. When targeting bigeye tuna, deep-set fishermen typically deploy ("set"), their gear in the morning, allowing it to fish ("soak") for several hours until the retrieval ("haul") begins around sundown. The hauling process may range from 4 to over 12 h, depending on the catch and amount of gear deployed.

We derived fishery-dependent data from two sources: "logbook" data recorded by vessel captains and "observer" data collected by on-board, independent fisheries observers. All deep-set captains are required to record and submit logbooks to NMFS which record the times and GPS coordinates of the start and finish of each set and haul of gear (i.e., four times and locations per fishing event), the number of hooks deployed, and counts of captured fish by species. Deep-set vessels are also required to carry a federal fisheries observer, if requested by NMFS, with a fleet-wide target coverage of 20% of trips per year. Observers collect detailed data on fishing operations, gear characteristics, and biological data from both target and nontarget catch. Observers monitor the entire haul-back of each gear deployment, identifying each captured species to the highest taxonomic level possible. Since 2009, observers also systematically measure to the nearest centimeter every third fish landed. Most bony fish are measured with standard fork length, while billfish are measured using an eye-fork measurement. Observers are also trained to classify and systematically record incidences of depredation. Evidence of odontocete depredation is distinct from other sources, such as squid or sharks, because toothed whales typically consume the whole fish up to the gill plates, leaving only the head attached to the hook (e.g., Secchi and Vaske 1998) (Fig. 1). False killer whales are also known to depredate bait from deep-set gear (Thode et al. 2016), but this is not systematically recorded by observers and is thus not considered or reported here. It is also likely that whales at times remove entire fish, in which case depredation may be underestimated or not recorded at all.

2.1.2. Overview of multistage modeling approach

We utilized a multistage modeling approach to estimate the total biomass of commercially important species lost to odontocete depredation in the deep-set fleet (see graphical overview in Fig. 2). We focused our analyses on bigeye tuna, yellowfin tuna (*Thunnus albacares*, Scombridae), and mahi-

Fig. 1. Examples of odontocete depredation on three commonly depredated catch species: (*a*) unidentified tuna species, (*b*) mahi-mahi, and (*c*) unidentified billfish. Note characteristic toothrakes and removal of body up to gill plates or jaws. Photo credit: NOAA Fisheries.

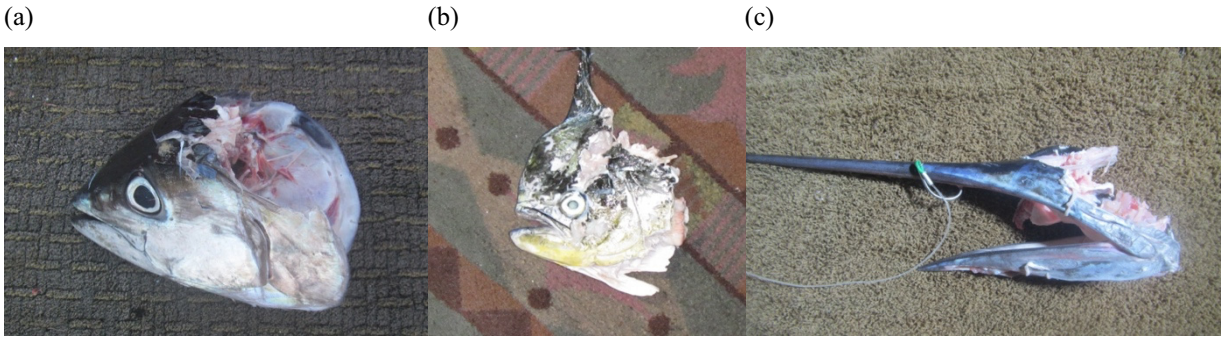

Fig. 2. Graphical schematic summarizing the major steps in the modeling approach used to derive predictions of depredated biomass across the fishery.

1) Build models of fish length for each species from observer-measured fish and relevant covariates.

Photo credit: NOAA Fisheries

2) Use these models to predict fish length for depredated fish. For tuna, also predict which tuna species the fish head is.

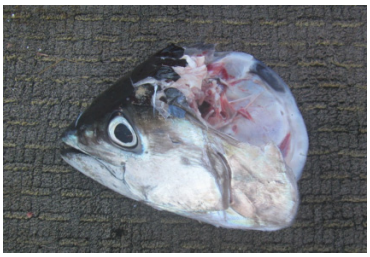

Photo credit: NOAA Fisheries

3) Apply length-weight relationship to estimate kg of each depredated fish.

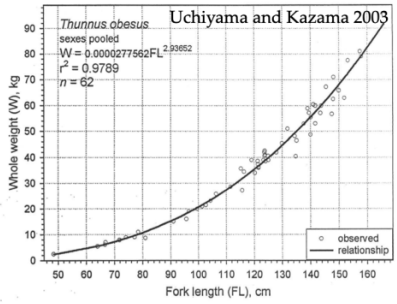

4) Aggregate the estimated biomass from individual fish for observed sets (observed effort shown below) in 5° x 5° x month cells and model the expected total biomass of depredated fish by species.

5) Use the best models of aggregated, depredated biomass to predict total depredated biomass for the entire fishery (i.e., extrapolating to unobserved fishing sets using logbook records).

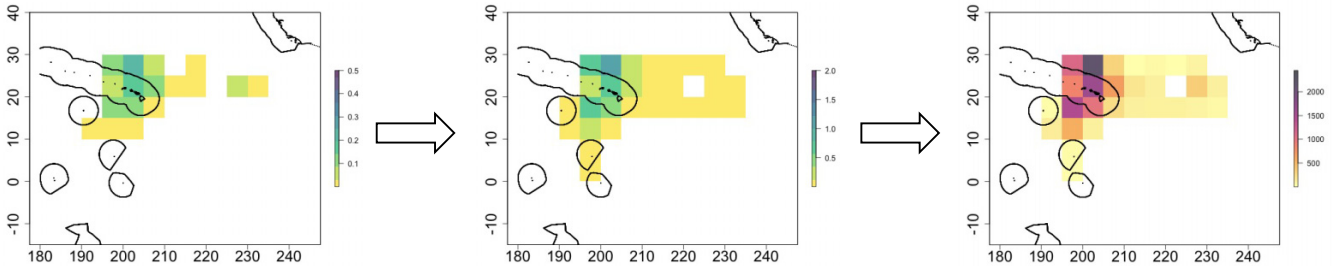

Observed effort January 2018 (millions of hooks)

Total (logbook) effort January 2018 (millions of hooks)

Total predicted biomass (kg) of bigeye tuna depredated in January 2018.

mahi (*Coryphaena hippurus*, Coryphaenidae). The tuna species caught in this fishery cannot be reliably distinguished from the head and gills of individual depredated fish, so we first modeled expected species identity for the two target tuna species (Stage 1). There is only one common species of mahi-mahi caught in this fishery and thus this step was only necessary for tuna. We then estimated the expected biomass of each depredated fish, by species, by modeling its expected length and calculating its expected mass from established length–weight relationships (Stage 2). We aggregated the estimated biomass from individual fish for all observed sets in 5° × 5° × month cells and modeled the expected total biomass of depredated fish by species on observed sets (Stage 3). Finally, we used the best models of aggregated depredated

biomass to predict total depredated biomass for the entire fishery (i.e., extrapolating to unobserved fishing sets using logbook records).

2.1.3. Derivation of covariates

We considered a suite of spatial, temporal, gear, operational, and/or environmental variables hypothesized to influence target species type, size, and/or aggregated depredated biomass, and included them in the three separate models corresponding to each stage (Stages 1, 2, and 3, respectively). Operationally, depth of gear has an important influence on both species and size composition of catch (Bigelow and Maunder 2007). As shoaling and concatenation of the main line makes it difficult to estimate the precise depth of gear directly (Bigelow et al. 2006), in both Stages 1 and 2 we utilized two gear-based variables that indicate the relative depth of an individually caught fish within a single set and relative to other sets. First, we calculated the standardized distance of each caught fish from the nearest float (HKDIST), such that a value of 0 is the first or last hook of the section, while a value of 0.5 is the very middle of the mainline between two successive floats. Due to the concatenation of mainline between floats, hooks closer to the middle point between two floats are expected to be deeper in the water than those near the float (Bigelow et al. 2006). Secondly, we used the number of hooks between floats for the entire fishing event (a parameter held constant as a boat deploys its gear across floats) as a general indicator of gear depth. More hooks between each float generally causes the gear to sink deeper (Bigelow et al. 2006).

We considered a range of static and dynamic environmental variables in all three stages including (detailed description and sources in Table 1) depth (DEP), sea surface temperature (SST), standard deviation of sea surface temperature (SSTDEV), the log of chlorophyll *a* concentration (CHLA), mixed layer depth (MLD), sea surface salinity (SAL), absolute dynamic topography (ADT), total kinetic energy (TKE), Oceanic Niño Index (ONI), and lunar phase (Stages 1 and 2 only). The first four covariates were extracted for the 2009–2018 study period using NOAA ERDDAP servers (https://coastwatch.pfeg.noaa.gov/erddap/index.html) and the rerddapXtracto package in RStudio statistical software, version 1.4.1103 (R Core Team 2018). MLD, SAL, ADT, and TKE for 2009–2018 were derived and processed from the EU Copernicus Marine Service (https://marine.copernicus.eu/). Spatial resolutions of the data ranged from 1/12° to 1/4° and temporal resolutions from days to months (Table 1).

For Stages 1 and 2, each environmental variable was associated with the spatial location of a single fishing set. As longlines can be tens of kilometers long, we derived the geographic centroid of each fishing set from the four observed spatial locations (set begin, set end, haul begin, and haul end) and then created a bounding box of 0.25° × 0.25° around the centroid point, which encompasses the average spatial footprint of observed sets of 250 km^2. For environmental variables of a resolution higher than 0.25° × 0.25°, we used nearest neighbor resampling to take the average value within this box for each set. Similarly, in Stage 3, we used nearest neighbor resampling to standardize covariates to the desired spatiotemporal resolution of 5° × 5° × month.

2.2. Modeling approach

2.2.1. Data preparations

We conducted detailed data explorations prior to model fitting for each Stage to identify appropriate inclusion of predictor variables. We assessed collinearity among explanatory variables by calculating Pearson correlation coefficients for all pairwise combinations of continuous variables, retaining only those with values less than 0.7 (Dormann et al. 2013). When two variables with similar ecological meaning were correlated, we retained the one with fewer missing values or a clearer ecological relationship to the response. We also plotted covariates in histograms, against response variables, and in residual plots from preliminary models.

2.2.2. Generalized additive modeling approach

We used variations of generalized additive models (GAMs) in each of the three Stages. GAMs are a regression approach that calculate smooth functions to estimate relationships between predictor and response variables (Wood 2017). The GAM approach allows flexibility in specifying different terms within a single model, with minimal a priori assumptions on the nature of each relationship (Wood 2017). They allow for a wide range of distribution families, so that diverse types of response variables can be accommodated (Zuur et al. 2009). A link function *g()* is used to relate a univariate response variable Y to a sum of smooth functions of the covariates X_i:

$$(1) \qquad g(E(Y)) = \alpha + \sum f_i(X_i)$$

where α is the intercept and f_i is a smooth function of the covariate X_i.

Following general approaches outlined in Zuur et al. (2009) and Dunn and Smyth (2018), for each species in each Stage, we began model selection from fully saturated models with cubic regression splines used for all univariate smoothers and tensor product smooths for any interaction terms. We used a cyclic cubic regression spline for a month to ensure a smooth step from December to January. Splines were implemented with a shrinkage parameter, which incorporates a penalty on the null space that drives the coefficients of noncontributing variables to zero (Wood 2006). These variables were removed after the first iteration, and then backward, stepwise selection was used on remaining variables to arrive at a final model (Zuur et al. 2009). All analyses were conducted in RStudio statistical software, version 1.2.5033 (R Core Team 2018). Stage 1 and 3 models were implemented with the package mgcv, version 1.8-31 (Wood 2006, 2007), and Stage 2 models were implemented using the gamm4 package, version 0.2-6 (Wood and Scheipl 2014). Further detail on each modeling Stage is provided below.

Table 1. Description of environmental covariates included in this study.

Covariate	Units	Data name and source	Original spatial resolution	Original temporal resolution
Depth (DEP)	m	General Bathymetric Chart of the Oceans (GEBCO) Grid[1]	15 arc sec	NA
Sea surface temperature (SST)	°C	NASA JPL Multi-scale Ultra-high Resolution (MUR) SST Analysis fv04.1[2]	0.01°	Daily
SST standard deviation (SSTDEV)	NA	NASA JPL Multi-scale Ultra-high Resolution (MUR) SST Analysis fv04.1b	0.01°	Daily
Chlorophyll *a* concentration (CHLA)	Natural log of $mg \cdot m^{-3}$	NASA Aqua MODIS Level 3[3]	4 km	Monthly
Mixed layer depth (MLD)	m	Global Ocean Physics Reanalysis GLORYS12V1[4]	1/12°	Daily
Surface salinity (SAL)	$1e^{-3}$	Global Ocean Physics Reanalysis GLORYS12V1	1/12°	Daily
Absolute dynamic topography (ADT)	m	Global ocean gridded L4 sea surface heights and derived variables reprocessed[5]	1/4°	Daily
Total kinetic energy (TKE)	$m^2 \cdot s^{-2}$	Global ocean gridded L4 sea surface heights and derived variables reprocessed	1/4°	Daily
Oceanic Niño Index (ONI)	NA	NWS Climate Prediction Center[6]	NA	3 month average
Lunar phase	NA	Package "lunar"[7]	NA	Daily

[1] https://coastwatch.pfeg.noaa.gov/erddap/info/GEBCO_2020/index.html
[2] https://coastwatch.pfeg.noaa.gov/erddap/info/jplMURSST41/index.html
[3] https://coastwatch.pfeg.noaa.gov/erddap/info/erdMH1chlamday/index.html
[4] https://resources.marine.copernicus.eu/product-download/GLOBAL_REANALYSIS_PHY_001_030
[5] https://resources.marine.copernicus.eu/product-download/SEALEVEL_GLO_PHY_L4_REP_OBSERVATIONS_008_047
[6] https://origin.cpc.ncep.noaa.gov/products/analysis_monitoring/ensostuff/ONI_v5.php
[7] https://cran.r-project.org/web/packages/lunar/lunar.pdf

2.2.3. Stage 1: predicting tuna species for unknown depredated tuna

Tuna caught in the Hawai'i deep-set fishery include bigeye, yellowfin, skipjack (*Katsuwonus pelamis*, Scombridae), and albacore (*Thunnus alalunga*, Scombridae) and these four species cannot be reliably identified from the head alone when depredation occurs. As the habitat preference of different tuna species varies spatially, temporally, and according to environmental and operational characteristics (e.g., depth of gear fished) (Bigelow and Maunder 2007; Arrizabalaga et al. 2015), we developed a multivariate classification model to predict the probability that each observed, odontocete-depredated tuna head was a particular tuna species. We utilized a GAM based on multinomial logistic regression, treating the species of tuna (one of four) as an unordered, categorical response variable. Covariates included the gear (i.e., depth) and environmental variables described above, as well as space (i.e., latitude and longitude coordinates) and time (month) to account for spatial, seasonal, and interannual variation in distributions of tuna species. We also included covariates for set-specific tuna species proportions, calculated as the number of each tuna species caught on the focal set divided by the total number of all tuna caught on that set.

We removed several candidate variables that were highly correlated with other variables or did not have noticeable discriminatory capability for the different species (i.e., the histogram distributions were nearly identical for each species). The resulting, fully saturated GAM was of the form:

$$\begin{aligned}(2)\quad \text{Tuna type} \sim\ & \beta_0 + s(\text{YFT\_prop}) + s(\text{SKJ\_prop}) \\ & + s(\text{ALB\_prop}) + s(\text{Longitude}) + s(\text{Latitude}) \\ & + c(\text{Month}) + s(\text{Year}) + s(\text{SST}) + s(\text{HKDIST})\end{aligned}$$

Multinomial GAMs produce p values that indicate the ability to discern each class from a base or reference class (in this case, bigeye tuna). For the four-class model, there were three sets of p values for each variable. To arrive at an optimal model, we utilized backwards, stepwise model selection, sequentially removing variables that were not significant for any of the three other tuna classes. We assessed model fit and prediction accuracy by fitting models to a training set of half the available data, and then testing those models on out-of-sample test data. We selected models with a higher specificity and/or lower AIC. The resulting best model was used to predict, for each individual depredated fish, the probability that it was each of the four species of tuna.

2.2.4. Stage 2: predicting depredated fish length

To derive estimates of the length (and ultimately biomass) of observed, depredated fish heads, we modeled the length of all intact (i.e., nondepredated), observer-measured fish for each of the three focal fish species and then used these models to predict fish length for depredated fish heads. We used fork length in centimeters for each fish species as a Gaussian-

family response variable with an identity link function. As the size of tuna in this fishery is known to vary operationally, seasonally, interannually, and geographically (Woodworth-Jefcoats and Wren 2020), we included as covariates the two gear/depth variables from Stage 1, a time/space interaction between month and the latitude and longitude of the centroid of the fishing event, consecutive month from 2009 to 2018, and the environmental covariates (Table 1). We included the presence or absence of depredation on the same set of the focal vessel as a categorical, parametric variable. Finally, we included set and trip ID as nested, random effects to control for variation within a single set and across individual trips. The final, saturated GAMs were of the form:

$$\begin{aligned}(3)\quad \text{Fish length}_{\text{species}} \sim \beta_0 + s(\text{Longitude, Latitude, Month}) + s(\text{Consecutive month}) + s(\text{HBF}) \\ + s(\text{HKDIST}) + s(\text{DEP}) + s(\text{SST}) + s(\text{SSTDEV}) + s(\text{CHLA}) + s(\text{MLD}) + s(\text{ADT}) + s(\text{TKE}) \\ + s(\text{ONI}) + s(\text{LUN}) + \text{Depredation} + \text{random}(\text{Set ID} \mid \text{Trip ID})\end{aligned}$$

For each species, we used model selection and cross-validation to arrive at the best candidate model of fish length for each species. We then applied these models to obtain expected length for each observed, depredated fish head encountered, then used published length–weight relationships to convert predicted lengths into predicted mass in kilograms (Uchiyama and Kazama 2003; Uchiyama and Boggs 2006).

We first removed all variables with a p value >0.1 and shrunken coefficients (expected degrees of freedom < 1). We then proceeded by removing the nonsignificant or the least significant covariates at each stage and refitting the model. We evaluated the prediction accuracy of candidate models at each stage using five-fold cross-validation, fitting each candidate model to five different slices of the data, each time leaving out one-fifth of the available data to test as novel data. We continued eliminating variables until we identified the model with the lowest average root mean squared error (RMSE) across the five folds, using the Akaike Information Criterion (AIC) to help decide between models in cases of very similar RMSE values.

GAMs allow various approaches for constraining the smoothness of individual variables to prevent overfitting. We left individual smoothed variables "unconstrained" for initial formulations of all saturated models. Following model selection, we tested whether assigning a "gamma" value, which constrains the flexibility of the model and counteracts overfitting by placing a heavier penalty on each degree of freedom (Wood 2007, 2017; Zuur et al. 2009), led to further increases in prediction accuracy (RMSE) for the best candidate model.

We used the best candidate model by species to predict the expected fork length for each observed, depredated fish head, and then used published length–weight relationships to convert predicted lengths into predicted mass in kilograms (Uchiyama and Kazama 2003; Uchiyama and Boggs 2006). For mahi-mahi, we summed the predicted depredated biomass into 5° × 5° × month strata. Given uncertainty in species identity for depredated tunas, we derived predicted biomass for both bigeye tuna and yellowfin tuna for every depredated tuna and assigned the predicted probability of tuna species from Stage 1 to each tuna head. We then resampled the data set 5000 times, randomly selecting at each iteration a species identity for each tuna head according to the predicted probabilities from the multinomial GAM. For each iteration we summed all bigeye and yellowfin tuna predicted biomass into 5° × 5° × month strata, and then chose the median biomass across the 5000 samples as the best estimate of that tuna species in each stratum.

2.2.5. Stage 3: predicting aggregated depredated biomass

We used GAMs to model the aggregated, predicted biomass depredated per species derived from Stages 1 and 2 (kg per 5° × 5° strata). Covariates considered included the environmental variables (Table 1), as well as year, month, and a year–month interaction term. We used the total number of observed hooks as an offset term to account for variations in sampling intensity in each strata (Zuur et al. 2009). Fully saturated models for each species were of the form:

$$\begin{aligned}(4)\quad \text{Catch removals (kg)} \sim \beta_0 + s(\text{Year, Month}) + s(\text{Year}) + s(\text{Month}) + s(\text{DEP}) + s(\text{SST}) + s(\text{SSTDEV}) + s(\text{CHLA}) + s(\text{MLD}) \\ + s(\text{ADT}) + s(\text{TKE}) + s(\text{ONI}) + s(\text{SAL}) + \text{offset}(\text{Number of hooks})\end{aligned}$$

Distributions of the response variable for each species indicated many zeros and overdispersion. We thus explored two different model formulations suited to these types of data. We first used a tweedie distribution with a log link function, which is a flexible, non-negative, continuous distribution that can accommodate large numbers of true zeros (Shono 2008; Zuur et al. 2009; Dunn and Smyth 2018). We also explored a two-stage, delta approach commonly used for

zero-inflated data sets (Shono 2008; Zuur et al. 2009; Sagarese et al. 2014). This approach involves first modeling the presence/absence of depredated biomass in each stratum using a binomial error distribution with a logit link function. A separate model is then used to model the conditional presence in nonzero strata. We used a gamma distribution with a log-link for the presence-only model.

Both model formulations (tweedie and delta-gamma) were carried through full model-selection and diagnosis processes. We conducted model selection as described in Stage 2, basing decisions of best models on the average RMSE on out-of-sample test data from five-fold cross-validation. We also tested whether including a gamma term improved prediction accuracy by restricting overfitting. The tweedie model formulations had the highest accuracy for each species and were used in subsequent prediction steps.

2.2.6. Predictions of depredation loss across the fishery

We used a catch standardization approach (e.g., Shono 2008; Tascheri et al. 2010; Mateo and Hanselman 2014) to estimate total depredated biomass across the fishery, using the best-selected, Stage 3 model for depredated biomass of each species derived from detailed observer data (~20% of effort), and then extrapolating across the fishery using total fishery effort from logbook data. To avoid inappropriate extrapolations in cases where cells had logbook but not observer data, we constrained predictions to only 5° × 5° strata that were within the range of individual environmental covariates present in the observed sets for each variable in the final model. We then summed these predictions into month and year summaries.

To quantify estimates of economic losses to depredation, we extracted data from the United Fishing Agency Auction in Honolulu, HI, where deep-set fishermen sell their catch following each trip. These data were publicly available from the United Fishing Agency Auction in 2019 (https://pop-hawaii.com/wp/), although they are no longer available from this location. The data include, for every day with auctioned fish catch from 2012 to 2018, the number of fish sold at auction, the total weight of fish sold that day, and the average price per pound. The data are separated into ahi (bigeye and yellowfin tuna) and "miscellaneous", which includes any other species sold at auction. We calculated the average price per pound per month for each category of fish and applied this value to the total biomass losses by month predicted by the GAM models.

2.2.7. Detection of depredation hotspots

We used the model predictions for bigeye tuna removals to calculate the average depredation per unit effort (DPUE) across the range of the fishery. This was done by summing the predicted biomass in kilograms and the total number of hooks fished in each stratum across all years, and then dividing the total biomass by the number of hooks for each 5° × 5° cell. We then mapped the predicted DPUE for each month to visualize depredation hotspots for bigeye tuna throughout the year across the range of the fishery.

3. Results

Between 2009 and 2018, a total of 182 525 sets were made on 13 465 trips by 169 unique vessels in the Hawai'i deep-set longline fishery. Observers were present on 20.8% of trips covering 20.4% of sets, providing a data set of 37 185 fishing events with detailed catch and depredation data. Approximately 85 different fish species were recorded as catch, although most species were encountered rarely. The top 10 caught species accounted for 87% of individually captured fish, and bigeye tuna and mahi-mahi accounted for nearly half of all retained fish (Table 2). Odontocete depredation on at least one captured fish was observed on 2394 (6.4%) of all observed sets. The number of fish depredated per set was right-skewed, with a median of 2 and a maximum of 63 depredated fish recorded on sets that experienced depredation. Approximately half of trips (48.4%) experienced odontocete depredation on at least one set and 22.6% experienced odontocete depredation on two or more sets. Observers recorded 9428 individual fish with damage from odontocete depredation, or around 1% relative to the total number of individual fish landed and kept for market. Tunas were the most commonly depredated fish (70%), followed by billfish (11%), wahoo (*Acanthocybium solandri*, Scombridae) (5%), and mahi-mahi (4%) (Table 2).

The selected model for the multinomial tuna discrimination analysis included the longitude and latitude of the centroid of the fishing set; year; month; the proportion of yellowfin, skipjack, and albacore tuna; and the standardized hook distance. The variables that showed the largest influence on species-discrimination were the proportion of species and hook distance (Fig. 3). Higher proportions of the overall less common tuna species (i.e., yellowfin, skipjack, and albacore) occurring on the same set were associated with a higher probability of occurrence for that species. In other words, the more individuals of a particular species that were positively identified on the same set, the more likely an unknown tuna species was also that same species (Figs. 3*a*–3*c*). Standardized hook distance, as a proxy for depth, was also influential for discriminating tuna species. Yellowfin and skipjack tuna, and to a lesser extent albacore, were more likely to be caught in shallower portions of the set compared to bigeye tuna (Figs. 3*d* and 3*e*).

The mean lengths of bigeye tuna, yellowfin tuna, and mahi-mahi were 111.9 cm (SD 23.1), 114.0 cm (SD 25.3), and 85.6 cm (SD 14.3), respectively. The length models that led to the best out-of-sample prediction included the interaction term between spatial location and month and the consecutive month term for each of the three focal species. The consecutive month variable indicated substantial interannual variation in predicted fish length for each species (Figs. 4*a*–4*c*). The size of bigeye tuna showed a decreasing trend over the 10 years assessed, but yellowfin and mahi-mahi did not show clear long-term trends. The optimal yellowfin tuna model additionally included terms for sea surface temperature and ONI, while the mahi-mahi model included sea surface temperature, ONI, and mixed layer depth (Figs. 4*d*–4*h*). Larger yellowfin tuna lengths were associated with more extreme ONI values, while the relationship between mahi-mahi length and ONI was less

Table 2. Fish species encountered in the Hawai'i deep-set tuna longline fishery during the study period (2009–2018).

	Total caught			Total kept			Total depredated		
	$n = 2\,152\,391$			$n = 1\,095\,661$			$n = 9428$		
	Species	Percentage of total	Cum. %	Species	Percentage of total	Cum. %	Species	Percentage of total	Cum. %
1	Longnose lancetfish (*Alepisaurus ferox*, Alepisauridae)	24	24	Bigeye tuna	35	35	Unidentified tuna (Scombridae spp.)	70	70
2	Bigeye tuna	19	43	Mahi-mahi	14	49	Unidentified billfish (Istiophoridae spp.)	11	81
3	Blue shark (*Prionace glauca*, Carcharhinidae)	8	51	Sickle pomfret (*Taractichthys steindachneri,* Bramidae)	12	62	Wahoo	5	86
4	Snake mackerel (*Gempylus serpens*, Gempylidae)	8	59	Skipjack tuna	6	68	Mahi-mahi	4	90
5	Mahi-mahi	8	66	Yellowfin tuna	6	74	Opah (Lampridae spp.)	3	93
6	Sickle pomfret	6	73	Escolar (*Lepidocybium flavobrunneum*, Gempylidae)	6	80	Unidentified pomfret (Bramidae spp.)	2	96
7	Escolar	5	78	Opah	4	85	Swordfish	1	96
8	Skipjack tuna	4	81	Wahoo	4	89	Unidentified bony fish	1	97
9	Yellowfin tuna	4	85	Shortbill spearfish (*Tetrapturus angustirostris*, Istiophoridae)	3	91	Longnose lancetfish	1	98
10	Opah	2	87	Albacore tuna	3	94	Escolar	1	99

Note: Observations are organized by species as percentage of total caught and identified, percentage of caught species that were landed and kept by vessels, and percentage by species depredated. Note certain depredated species are combined into taxonomic categories to account for the difficulty of identifying remains of these taxa.

Fig. 3. Statistical relationships between covariates and discrimination of three tuna species from bigeye tuna in multinomial GAM. Plots (*a*, *d*) represent discrimination of skipjack tuna from bigeye, (*b*, *e*) yellowfin from bigeye, and (*c*, *f*) albacore from bigeye. *y*-axes are transformed to the probability scale to represent the expected probability of each species at particular covariate values. Distributions of observed values are indicated by a rug plot along each *x*-axis. Shading reflects 2× standard error curves. See Table 1 for descriptions of environmental covariates.

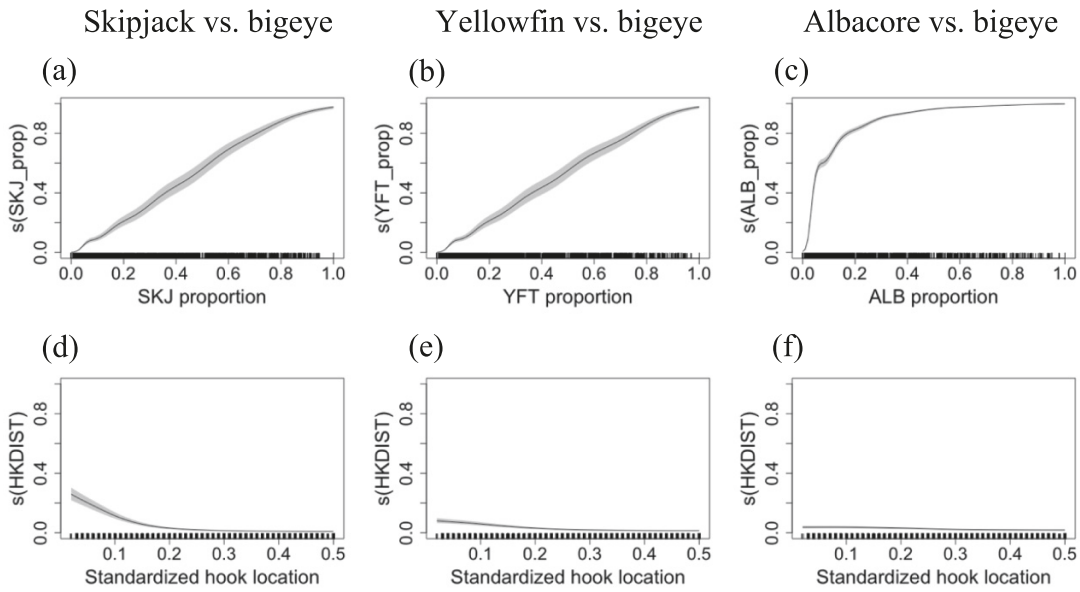

clear. Conversely, mahi-mahi showed a clear positive relationship between length and sea surface temperature, while the relationship with yellowfin tuna was less clear. There was a slight unimodal relationship between mahi-mahi length and mixed layer depth, with the largest mahi-mahi associated with mixed layer depths of around 40 m. For bigeye tuna, several variables that were considered significant in the GAMs ($p < 0.01$) were dropped during model selection, as remov-

Fig. 4. Statistical relationships between covariates and fork length (cm) for three target fish species. Plots (*a*–*c*) indicate the relationship between fish size and consecutive month for bigeye tuna (*a*), yellowfin tuna (*b*), and mahi-mahi (*c*) over the study period. Plots (*d*, *e*) and (*f*–*h*) indicate additional environmental covariates included in best-fit models for yellowfin tuna and mahi-mahi, respectively. *y*-axes are of the same scale to facilitate comparisons of variable importance on length for each species. Distributions of observed values are indicated by a rug plot along each *x*-axis. Shading reflects 2× standard error curves. See Table 1 for descriptions of environmental covariates.

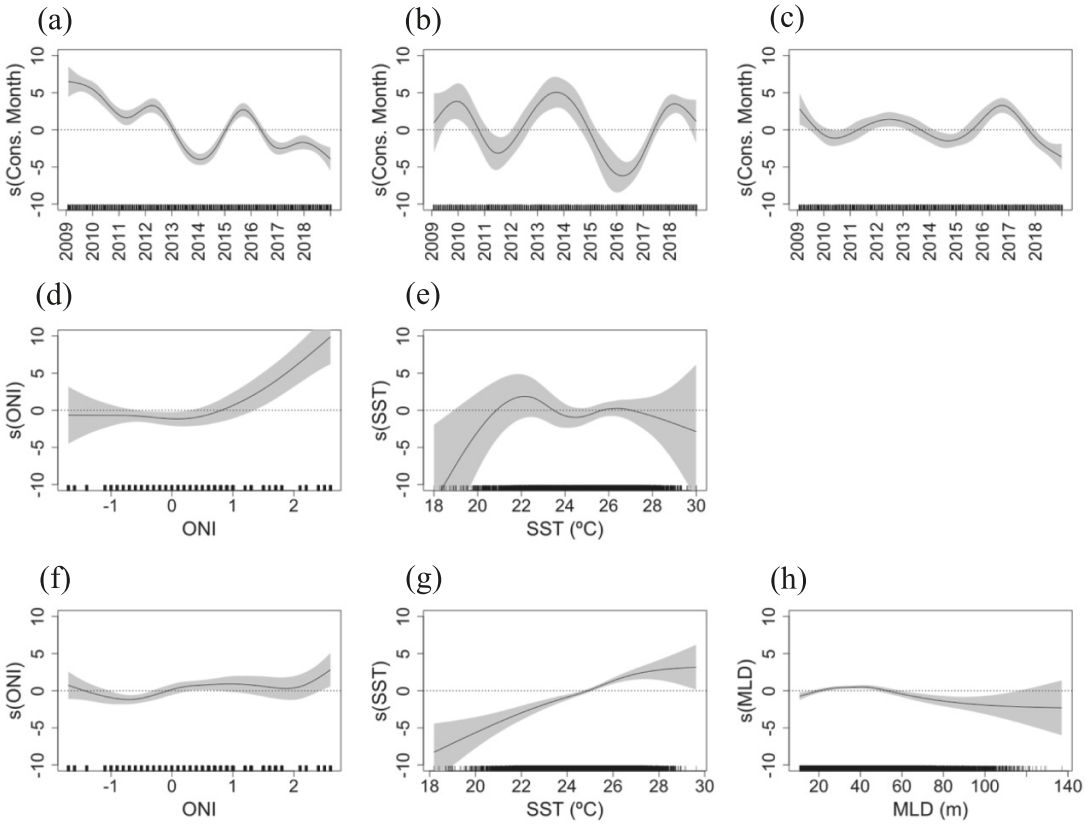

ing them led to increased prediction accuracy. These included ONI, sea surface index, standardized hook distance, and the presence of marine mammal depredation on the same set.

Depredation of bigeye tuna occurred in 34% of 5° × 5° × month strata for which fishing effort was observed. In strata with depredation, the mean estimated biomass of depredated bigeye tuna was 179.5 kg (SD 225.4) per cell per month. Yellowfin tuna were depredated in 13% of observed strata with a mean of 94.4 kg (SD 117.0) when present. Mahi-mahi were depredated in 11% of observed strata with mean of 9.3 kg (SD 7.1) when present. GAMs with a tweedie error distribution for the response variable and a log link had comparably higher prediction accuracy for each species than the two-step delta-gamma models. The best selected models for bigeye tuna, yellowfin tuna, and mahi-mahi had explained deviances of 18%, 32%, and 18%, respectively, which is reasonable in comparison to other catch-standardization analyses (Tascheri et al. 2010). All three included the single temporal covariates year and month (Fig. 5), while the interaction between year and month was also included for both yellowfin tuna and mahi-mahi (not shown). All three species showed lower levels of depredation north of the equator in summer months, although this was most pronounced for bigeye tuna and mahi-mahi (Figs. 5*b*, 5*f*, and 5*m*). The bigeye tuna model indicated a variable and slightly positive relationship between predicted depredation and seafloor depth and a nearly linear, positive relationship with sea surface temperature (Figs. 5*c* and 5*d*). The yellowfin tuna model included the environmental covariates depth, chlorophyll *a* concentration, salinity, ADT, and TKE (Figs. 5*g*–5*k*); and the best mahi-mahi model included ADT and mixed layer depth (Figs. 5*l*–5*o*). Some of these patterns were relatively weak or showed variable and unclear relationships, while others were clearer. Yellowfin tuna and mahi-mahi depredation levels had clear positive associations with ADT (Figs. 5*j* and 5*o*). The significant effect between yellowfin depredation and salinity showed a mostly flat relationship with a sharp decline at high salinity levels (Fig. 5*i*).

The predicted mean annual depredated biomass of bigeye tuna, yellowfin tuna, and mahi-mahi from 2009–2018 was 78.2 t (52.3–104.0), 15.8 t (5.8–25.7), and 1.3 t (0.7–1.9), respectively, or 95.2 t (58.8–131.7) per year in aggregate (Fig. 6*a*). The average annual estimated cost across all three species from 2012 to 2018 was $1 117 000 USD ($694 000–$1 541 000) (Fig. 6*b*). On an operational scale, sets that experienced odontocete depredation lost a predicted (median) volume of 55.2 kg (52.0–57.9) of bigeye and yellowfin tuna, corresponding to a median cost of $579 USD ($549–$614). The median

Fig. 5. Statistical relationships between select covariates and predicted depredation (kg) for three target fish species. Plots (*a*–*d*) indicate the relationship between predicted bigeye tuna catch removals, plots (*e*–*k*) show relationships for yellowfin tuna, and plots (*l*–*o*) for mahi-mahi. *y*-axes are of the same scale to facilitate comparisons of variable importance for each species. Distributions of observed values are indicated by a rug plot along each *x*-axis. Shading reflects 2× standard error curves. See Table 1 for descriptions of environmental covariates.

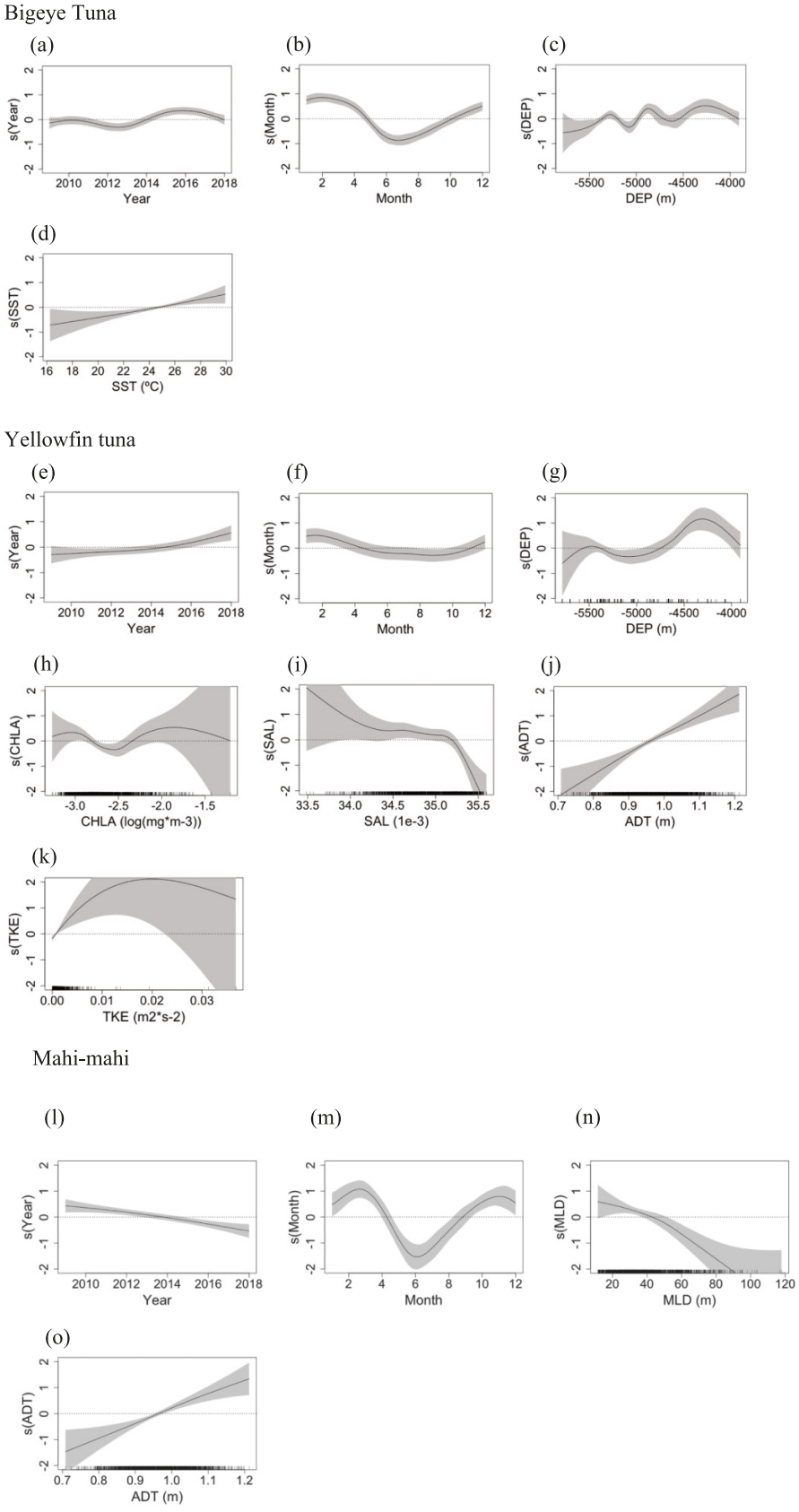

Fig. 6. Predicted annual biomass lost by species (*a*) and total economic costs (*b*) resulting from catch removals by odontocetes in the deep-set fishery. Error bars indicate 95% confidence intervals. Also displayed is the total number of hooks set annually across the entire deep-set longline fishery (*c*).

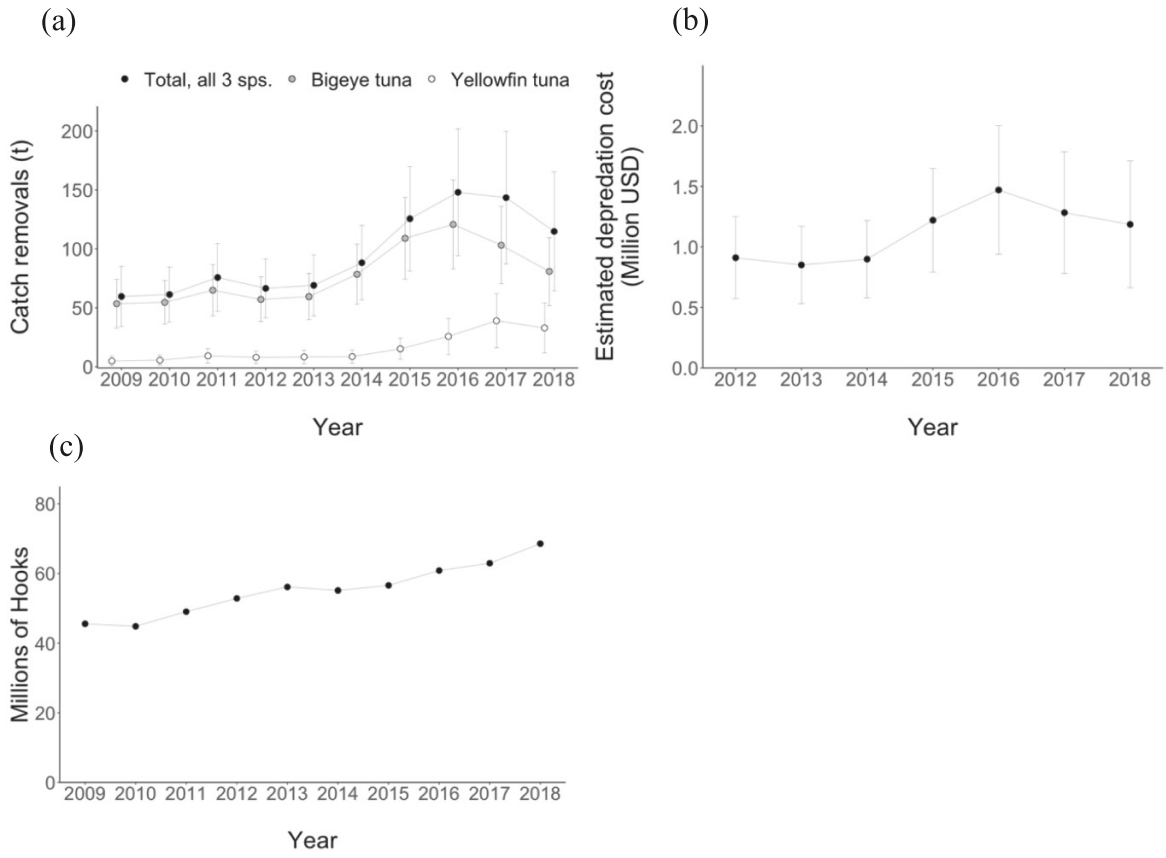

predicted bigeye and yellowfin tuna catch removal on trips that experienced depredation at least once was 88.0 kg (83.7–92.9 kg) corresponding to $921 USD ($871–$971).

Predicted catch removal rate or DPUE (kg depredated fish/fishing effort) for bigeye tuna was averaged across years and mapped for each 5° × 5° × month strata to visualize relative depredation rates over the year (Fig. 7). Predicted bigeye tuna depredation rates were highest in the first and last quarters (November–April) and in the southwestern regions of the fishery. Depredation rates were lowest in the summer months (June–August). Total depredation rate of all three species combined and rates for yellowfin tuna and mahi-mahi separately are shown in Supplementary Material, Fig. S3.

4. Discussion

We used a multistage, tiered modeling approach to derive quantitative estimates of catch losses by depredating odontocetes in the Hawai'i deep-set longline tuna fishery. Depredation is relatively rare and variable on a per-set basis, but lost catch and economic costs can be substantial when they do occur. Similarly, the intensity of depredation varies in time and space, but exceeded 100 t and 1 million USD in estimated costs to the fleet in each of the last four study years (2015–2018). These values are likely underestimates as fish entirely removed by the whales cannot be counted and we do not have a good estimate of the rate at which entire fish are lost or consumed. Our findings demonstrate the broad-scale significance of odontocete depredation in this fishery and help quantify the ecological and economic implications of this interaction.

4.1. Depredation patterns

Most observed, depredated fish were either target or nontarget species commonly retained for sale. The estimated rates of occurrence of depredation on a per-set and per-trip level in this study are consistent with previous assessments of this fishery (Forney et al. 2011; Fader et al. 2021). Forney reported a nearly identical set-level depredation rate of 6% extending back to 2003. Summaries of catch rates by species, including depredated fish, have also been reported for this fishery and are largely consistent with the present study (Oleson et al. 2010; Fader et al. 2021). As shown here, tuna are consistently observed as the most frequently depredated species, but odontocetes consume a range of commonly caught (and marketable) species including mahi-mahi, wahoo, and billfish. Most species were depredated at rates that were proportional to their composition of total catch, although some were depredated infrequently relative to their overall catch rates (Table 2). For example, sharks, although a common nontarget catch in this fishery, are virtually

Fig. 7. Predicted bigeye tuna depredation rates (kg bigeye tuna removed/1000 hooks set) averaged by month across the 10 study years (2009–2018). The scale is the same for each month, with the darkest purple corresponding to the highest observed depredation rate across all months (4.28 kg/1000 hooks). The USA Exclusive Economic Zone around Hawai'i, California, and U.S. territories are depicted with a black line.

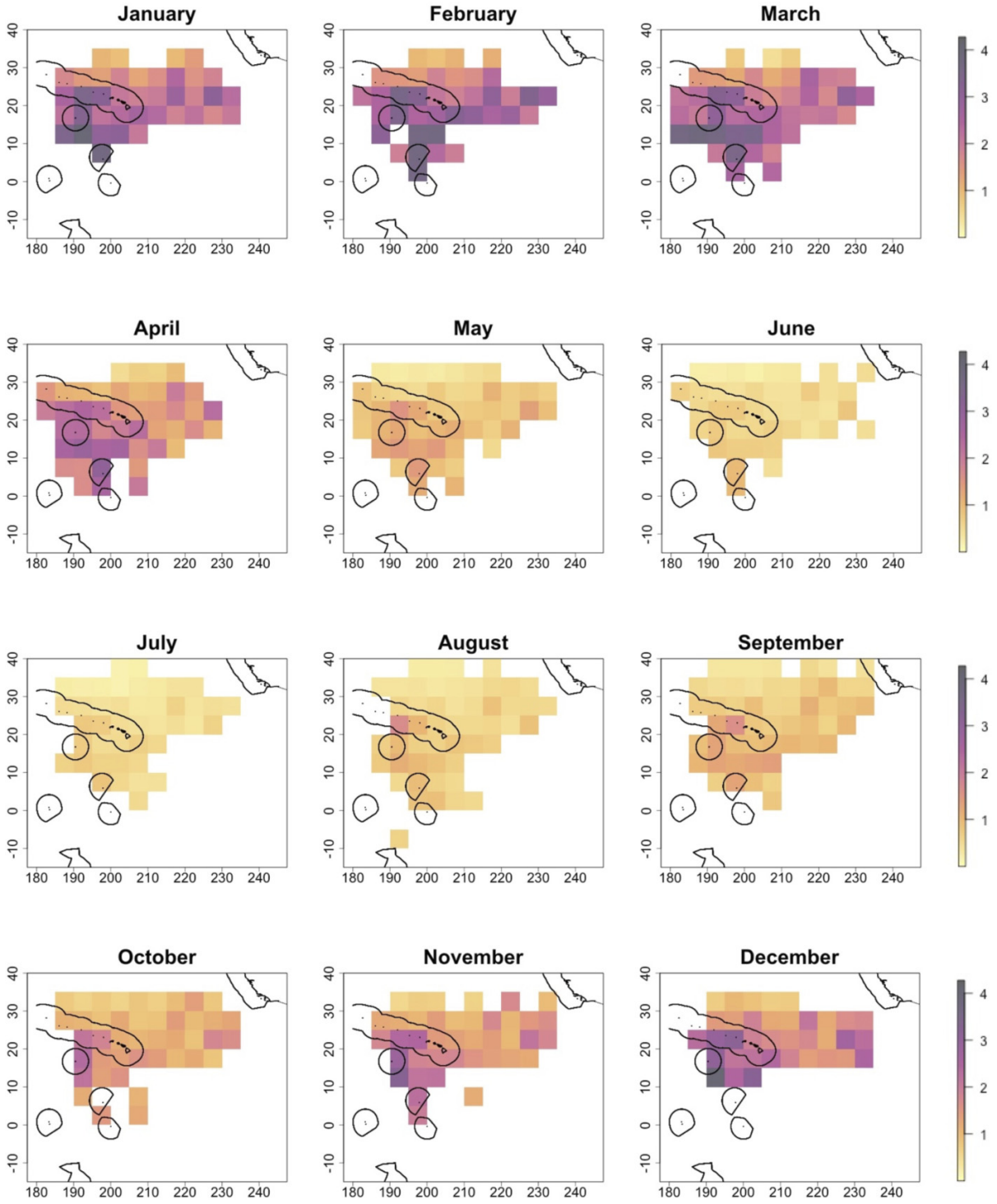

never depredated. Depredation on the longnose lancetfish (*Alepisaurus ferox*, Alepisauridae) was also rare, even though it was the most commonly caught species. This may be, at least in part, due to the gelatinous nature of their flesh, which makes it difficult for observers to categorize the source of damage for this discard species.

Despite the detailed observations of depredation described here, there were notable challenges in scaling up from observed fish remains to biomass estimates from the observer-collected data set. Odontocetes typically depredate the entire body of the fish, leaving behind only the jaws and gills. Some species, such as mahi-mahi, are still identifiable when depre-

dated. Tuna are more challenging, as several species are regularly caught and cannot be reliably distinguished by the head alone. We used multinomial GAMs to account for uncertainty in tuna species identification when aggregating predicted catch removals by species. The models provided strong out-of-sample classification accuracy on known tuna species, with the strongest predictors based on the proportion of species for positively identified, nondepredated fish as well as the relative depth of the set. Of note, bigeye tuna is more commonly caught on deeper gear than the next two most common tuna species, yellowfin, and skipjack. By utilizing this approach, we identified the most likely species to occur based on general catch trends and known operational characteristics, while incorporating the uncertainty in positive species identification. We note that there are reliable and low-cost molecular assays that can discriminate tuna and other fish species with high accuracy (Michelini et al. 2007). Incorporating tissue collection from tuna heads by observers is thus one opportunity to further refine the accuracy of this approach.

An additional layer of complexity is that observers do not collect morphometric measurements of depredated fish remains that could be used to estimate the intact size of the fish. Bigeye tuna caught in this fishery range from 27 to 205 cm, and there is considerable variation in the size of captured fish seasonally, interannually, and geographically (Woodworth-Jefcoats and Wren 2020). Developing an allometric relationship between fish remains and intact fish size, and any necessary data collection protocols (e.g., observers measuring fish remains on the vessel or photographing them to conduct later image analysis), is thus a clear opportunity to improve the approach described here. Without such data, we relied on model reconstructions of depredated fish size. Since 2009, observers have systematically recorded the length of every third landed fish, providing a robust data set of fish lengths for undamaged fish caught concurrently or in similar environmental conditions. We used this data set to develop models predicting fish length for each focal species based on spatial, temporal, operational, and environmental covariates. Space and time covariates were important in models for each species and indicated a likely cohort and recruitment structure with interannual peaks in body size, as has been observed in other studies in the region (Woodworth-Jefcoats and Wren 2020).

Our approach assumes that depredated tuna and mahi-mahi are otherwise equivalent to nondepredated, measured fish of the same species (i.e., individual fish are equally likely to be selected by a depredator regardless of size). It is possible that predators could preferentially select either smaller or larger fish, for example due to easier handling (smaller fish) or increased likelihood of detection and/or larger reward of capture (larger fish). Either scenario would bias estimates of fish length for depredated fish, because any remaining nondepredated fish on a depredated set, would, on average and all else equal, likely be larger (in case of a preference for small fish) or smaller (in case of a preference for large fish) than fish of the same species on nondepredated sets. To address this possibility, we incorporated a binary variable in the starting models for fish length indicating whether odontocete depredation occurred on the same set.

The variable for presence of depredation was not included in the best-predicting model for any of the three species, although it was statistically significant and one of the last variables to be removed from the bigeye tuna models during model selection. The direction of the effect suggested that nondepredated, measured bigeye tuna were slightly larger on sets where depredation did not occur. There are at least two mechanisms that could explain this pattern. It is possible that depredation occurs more commonly on sets where the fishery catches smaller tuna on average. This could be driven by space and time patterns of fishery effort and depredation occurrence, for example, if fish were larger in northern areas where the fishery experiences lower depredation rates (Forney et al. 2011; Fader et al. 2021). The space, time, and/or environmental covariates would likely account for this pattern however, rather than a categorical predictor of depredation. An alternative explanation is that depredators are more likely to consume larger fish when they encounter a set, and thus any remaining, nondepredated fish on that set, which are the only ones available to be measured, are smaller than would otherwise be expected. False killer whales are known to attack and consume large, pelagic fish such as tunas, mahi-mahi, swordfish, and billfish in the wild (Baird et al. 2008; Baird 2009). There is little reason to suspect that this large predator would preferentially select smaller fish, and indeed, consuming hooked and restrained fish may allow them to consume even larger fish than they could capture if the prey was free swimming. This hypothesis also aligns with reports by fishermen suggesting that whales prefer to depredate large ahi tuna (TEC Inc. 2009). Thus, this pattern may suggest a slight underestimate of depredated fish length and negatively bias the aggregated estimates of depredated biomass. Nonetheless, an effect in either direction is likely to be small, as the statistical effect of larger fish on nondepredated sets was approximately a 1 cm difference.

The final step to estimate levels and patterns of depredation across the fishery was to scale estimates of catch removal from the observed data set, representing approximately 20% of total deep-set effort, to the entire fleet. We utilized a catch standardization approach, commonly used in stock assessment analyses to estimate abundance from CPUE data (e.g., Shono 2008; Tascheri et al. 2010; Mateo and Hanselman 2014), to model depredation per effort relative to covariates and then predict biomass of depredated fish in areas with only effort and covariate data. This approach allowed estimates of catch removals for focal species across the fishery, as well as identification of potential hotspots of higher depredation risk. Several environmental covariates were influential in predictions for each species. Bigeye tuna catch removals increased with increasing sea surface temperature, which is consistent with anecdotal reports of fishermen suggesting that depredation is less likely in waters cooler than 67 °F–68 °F (~19 °C –20 °C) (TEC Inc. 2009). Depredation intensity was positively associated with ADT for both yellowfin tuna and mahi-mahi, which is consistent with observations in Fader et al. (2021) that the probability of depredation is lower when fishing in waters with lower ADT values.

Predicted depredation intensity for bigeye tuna, aggregated by month across the 10 years of the study, indicated

the highest rates of total bigeye catch removals from odontocete depredation in the first and last quarters of the year (Figs. 5*b* and 7). There were also apparent spatial hotspots in the southwest and, to a lesser extent, the northeastern areas of the fishery, while depredation rates were low in the northernmost parts of the fishery in all months. These patterns are consistent with previous quantitative assessments, which have indicated relatively lower depredation rates north of the equator in summer months when the fleet fishes farther to the north (Forney et al. 2011; Fader et al. 2021), as well as anecdotal information from fishermen who have reported potential depredation hotspots in the south and southwest portions of the fishery (TEC Inc. 2009).

4.2. Catch removals and implications

The present study suggests that depredation is relatively rare on a per-set basis, but when it occurs, it can result in high rates of lost catch on individual fishing sets or trips. The median estimated cost, when depredation occurs on a set, was just under $600 USD, although the worst 10% of depredated sets experienced estimated losses of more than $2300 USD. The worst 10% of depredated trips exceeded $3500 in estimated losses. Due to the long durations and great distances traveled to reach fishing grounds, costs are already high in the Hawai'i longline fishery, regularly exceeding $30 000 per trip (Chan and Pan 2021). The prospect of losing several thousands of dollars in a single day of fishing is thus understandably a significant concern for longline fishermen. These estimates also do not account for additional costs of depredation that are difficult or impossible to quantify, such as bait lost to depredating whales or wasted on depredated fish. There are also opportunity costs such as lost gear, crew and vessel time, and costs likely incurred to make up for lost catch, as observed in other fisheries subject to odontocete depredation (Gilman et al. 2007; Peterson et al. 2014; Tixier et al. 2020*a*).

When considered in aggregate, total losses to depredation by odontocetes may be economically and ecologically meaningful. We estimate that between 100–150 t and over 1 million USD in losses of the three focal species were incurred in each of the last 4 years of the study period, mostly due to depredation on bigeye tuna. For context, over these same 4 years (2015–2018) the total bigeye tuna catch averaged 3384 t per year (WCPFC 2019) and the total revenue of the fishery averaged 97 million USD per year (WPRFMC 2022). The Hawai'i longline fishery also operates on regional catch limits for bigeye tuna set by two Regional Fisheries Management Organizations (RFMOs): the Inter-American Tropical Tuna Commission in the Eastern Pacific Ocean and the Western and Central Pacific Fisheries Commission (WCPFC). The fishery experienced partial closures in each of the 10 study years by reaching catch limits (Ayers et al. 2018). If catch removals from depredation were included in stock assessments, these limits would be reached more quickly, and the additional effort to account for depredated catch removals may indirectly increase fishing pressure on target stocks. The total annual loss of 100–150 t may seem relatively small on an ocean-basin scale in which 72 391 t of bigeye tuna was caught by longlines in 2019 in the WCPFC area alone, but the Hawai'i fishery accounts for only 5% of total landed bigeye in the Central Pacific Ocean (WCPFC 2019). If this analysis was extended to all fishing effort managed by these two RFMOs, the scale of catch losses caused by odontocete depredation could be sufficiently large to warrant inclusion in stock assessments.

Finally, we documented an increase in catch removals and associated economic losses over the study period. Much of this increase is undoubtedly due to the increase in fishing effort observed in the fishery (Fig. 6*c*). The peak in 2016–2017 does not seem to be entirely explained by aggregate fishing effort, however, and corresponds to an evident increase in depredation rates for bigeye tuna (Fig. 5*a*). Interestingly, yellowfin tuna and mahi-mahi depredation rates show distinct patterns over the decade, with a small increase in yellowfin since 2016 and a general decline in the depredation rate for mahi-mahi (Figs. 5*e* and 5*l*). It is unclear whether these patterns were driven by changes in distributions or behaviors of target species, odontocetes, the fishery itself, or some combination of these factors.

5. Conclusions

This study used a novel approach for estimating catch removals from odontocete depredation in longline fisheries and identifying hotspots of depredation activity. We utilized a rich data set of unbiased observations of catch and the occurrence of depredation to derive minimum estimates of catch removals by odontocetes across the fishery. We also took advantage of the fact that there is a single auction in which the vast majority of Hawai'i deep-set fish are sold, allowing us to estimate the price fishermen would have received had they landed and sold depredated fish at that time.

There are some important limitations and assumptions in our modeling applications. Some of these could be addressed by improvements in observer coverage and observer data collection protocols (e.g., collecting tissue samples for depredated species identification and morphometric measurements to estimate depredated fish size). Nonetheless, the estimates of loss derived here can help fishery managers and fishermen to better understand the economic and ecological consequences of depredation and inform mitigation strategies by helping to understand drivers and predictors of depredation patterns at large spatial and temporal scales. Such information is important for improving ecosystem-based fisheries management and refining stock assessments to account for mortality of target species caused from depredation. This approach is also adaptable and scalable to other fisheries that experience depredation and demonstrates the importance of detailed observer data to document and contextualize patterns of relatively rare, but important, events such as depredation and bycatch.

Acknowledgements

We thank the Pacific Islands Regional Observer Program, especially fisheries observers, who collect the data essential for documenting patterns of depredation and bycatch in Hawai'i

longline fleets. We thank C. Guinet for contributing to early discussions about the methods and for providing resources and office space to JEF while conducting parts of the analysis for the manuscript. We thank the CJFAS editorial team and three anonymous reviewers for helpful feedback on this manuscript. A version of this work appears in JEF's Ph.D. Dissertation (Fader 2022).

Article information

History dates

Received: 10 July 2022
Accepted: 11 February 2023
Accepted manuscript online: 1 March 2023
Version of record online: 3 April 2023

Copyright

Data availability

Longline fishery logbook and observer data are restricted due to confidentiality requirements. They are available only through nondisclosure agreements with NOAA. The auction data are available from the United Fishing Agency.

Author information

Author ORCIDs

Joseph E. Fader https://orcid.org/0000-0002-9115-6099

Author contributions

Conceptualization: JEF, JAM, AJR
Data curation: JEF
Formal analysis: JEF, RSS
Funding acquisition: JEF
Investigation: JEF, JAM, RSS, AJR
Methodology: JEF, JAM, RSS, AJR
Project administration: JEF
Resources: JAM, AJR
Supervision: RSS, AJR
Writing – original draft: JEF
Writing – review & editing: JEF, JAM, RSS, AJR

Competing interests

The authors declare there are no competing interests.

Funding information

We gratefully acknowledge funding support for JEF from the National Oceanic and Atmospheric Association's (NOAA) and the Duke University Graduate School. This project received funding under award (NA17NMF4720261) from NOAA Fisheries Service, in cooperation with the Bycatch Reduction Engineering Program (BREP). The statements, findings, conclusions, and recommendations are those of the authors and do not necessarily reflect the views of NOAA Fisheries.

Supplementary material

Supplementary data are available with the article at https://doi.org/10.1139/cjfas-2022-0156.

References

Anderson, D., Baird, R.W., Bradford, A.L., and Oleson, E. 2020. Is it all about the haul? Longline fishery interactions and spatial use by pelagic false killer whales in the central North Pacific. Fish. Res. **230**: 105665. doi:10.1016/j.fishres.2020.105665.

Arrizabalaga, H., Dufour, F., Kell, L., Merino, G., Ibaibarriaga, L., Chust, G., et al. 2015. Global habitat preferences of commercially valuable tuna. Deep Sea Res. Part II Top. Stud. Oceanogr. **113**: 102–112. doi:10.1016/j.dsr2.2014.07.001.

Ayers, A.L., Hospital, J., and Boggs, C. 2018. Bigeye tuna catch limits lead to differential impacts for Hawai'i longliners. Mar. Policy, **94**: 93–105. doi:10.1016/j.marpol.2018.04.032.

Baird, R.W. 2009. A review of false killer whales in Hawaiian waters: biology, status, and risk factors. Report prepared for the U.S. Marine Mammal Commission under Order No. E40475499. Cascadia Research Collective.

Baird, R.W., Gorgone, A.M., McSweeney, D.J., Webster, D.L., Salden, D.R., Deakos, M.H., et al. 2008. False killer whales (*Pseudorca crassidens*) around the main Hawaiian Islands: long-term site fidelity, inter-island movements, and association patterns. Mar. Mammal Sci. **24**: 591–612. doi:10.1111/j.1748-7692.2008.00200.x.

Bayless, A.R., Oleson, E.M., Baumann-Pickering, S., Simonis, A.E., Marchetti, J., Martin, S., and Wiggins, S.M. 2017. Acoustically monitoring the Hawai'i longline fishery for interactions with false killer whales. Fish. Res. **190**: 122–131. doi:10.1016/j.fishres.2017.02.006.

Bigelow, K., Musyl, M.K., Poisson, F., and Kleiber, P. 2006. Pelagic longline gear depth and shoaling. Fish. Res. **77**: 173–183. doi:10.1016/j.fishres.2005.10.010.

Bigelow, K.A., and Maunder, M.N. 2007. Does habitat or depth influence catch rates of pelagic species? Can. J. Fish. Aquat. Sci. **64**: 1581–1594. doi:10.1139/f07-115.

Blasi, M.F., Giuliani, A., and Boitani, L. 2015. Influence of trammel nets on the behaviour and spatial distribution of bottlenose dolphins (*Tursiops truncatus*) in the Aeolian Archipelago, Southern Italy. Aquat. Mamm. **41**: 295–310. doi:10.1578/AM.41.3.2015.295.

Boggs, C.H., and Ito, R.Y. 1993. Hawaii's pelagic fisheries. Mar. Fish. Rev. **55**: 69–82.

Branch, T.A., Watson, R., Fulton, E.A., Jennings, S., McGilliard, C.R., Pablico, G.T., et al. 2010. The trophic fingerprint of marine fisheries. Nature, **468**: 431–435. doi:10.1038/nature09528. PMID: 21085178.

Chan, H.L., and Pan, M. 2021. Fishing trip cost modeling using generalized linear model and machine learning methods – A case study with longline fisheries in the Pacific and an application in Regulatory Impact Analysis. PLoS ONE **16**: e0257027. doi:10.1371/journal.pone.0257027. PMID: 34492086.

Dormann, C.F., Elith, J., Bacher, S., Buchmann, C., Carl, G., Carré, G., et al. 2013. Collinearity: a review of methods to deal with it and a simulation study evaluating their performance. Ecography, **36**: 27–46. doi:10.1111/j.1600-0587.2012.07348.x.

Dunn, P.K., and Smyth, G.K. 2018. Generalized linear models with examples in R. Springer.

Esteban, R., Verborgh, P., Gauffier, P., Giménez, J., Guinet, C., and De Stephanis, R. 2016. Dynamics of killer whale, bluefin tuna and human fisheries in the Strait of Gibraltar. Biol. Conserv. **194**: 31–38. doi:10.1016/j.biocon.2015.11.031.

Fader, J.E. 2022. Patterns of odontocete depredation and bycatch in pelagic longline fisheries. Ph.D., Duke University, Ann Arbor.

Fader, J.E., Baird, R.W., Bradford, A.L., Dunn, D.C., Forney, K.A., and Read, A.J. 2021. Patterns of depredation in the Hawai'i deep-set longline fishery informed by fishery and false killer whale behavior. Ecosphere, **12**: e03682. doi:10.1002/ecs2.3682.

Federal Register. 2010. Taking of Marine Mammals Incidental to Commercial Fishing Operations; False Killer Whale Take Reduction Plan – Proposed Rule. Federal Register 76 FR 42082: Washington, DC. pp. 42082–42099.

Forney, K., and Kobayashi, D. 2007. Updated Estimates of Mortality and Injury of Cetaceans in the Hawaii-based Longline Fishery, 1994-2005. U.S. Dept. of Commerce, NOAA Technical Memorandum NOAA-TM-NMFS-SWFSC-412.

Forney, K.A., Kobayashi, D.R., Johnston, D.W., Marchetti, J.A., and Marsik, M.G. 2011. What's the catch? Patterns of cetacean bycatch and depredation in Hawaii-based pelagic longline fisheries. Mar. Ecol. **32**: 380–391. doi:10.1111/j.1439-0485.2011.00454.x.

Gilman, E., Brothers, N., McPherson, G., and Dalzell, P. 2007. A review of cetacean interactions with longline gear. J. Cetacean Res. Manag. **8**: 215.

Gilman, E., Clarke, S., Brothers, N., Alfaro-Shigueto, J., Mandelman, J., Mangel, J., et al. 2008. Shark interactions in pelagic longline fisheries. Mar. Policy, **32**: 1–18. doi:10.1016/j.marpol.2007.05.001.

Guerra, A.S. 2019. Wolves of the sea: managing human-wildlife conflict in an increasingly tense ocean. Mar. Policy, **99**: 369–373. doi:10.1016/j.marpol.2018.11.002.

Guinet, C., Tixier, P., Gasco, N., and Duhamel, G. 2015. Long-term studies of Crozet Island killer whales are fundamental to understanding the economic and demographic consequences of their depredation behaviour on the Patagonian toothfish fishery. ICES J. Mar. Sci. **72**: 1587–1597. doi:10.1093/icesjms/fsu221.

Hamer, D.J., Childerhouse, S.J., and Gales, N.J. 2012. Odontocete bycatch and depredation in longline fisheries: a review of available literature and of potential solutions. Mar. Mamm. Sci. **28**: E345–E374. doi:10.1111/j.1748-7692.2011.00544.x.

Hanselman, D.H., Pyper, B.J., and Peterson, M.J. 2018. Sperm whale depredation on longline surveys and implications for the assessment of Alaska sablefish. Fish. Res. **200**: 75–83. doi:10.1016/j.fishres.2017.12.017.

Lewison, R.L., Crowder, L.B., Read, A.J., and Freeman, S.A. 2004. Understanding impacts of fisheries bycatch on marine megafauna. Trends Ecol. Evol. **19**: 598–604. doi:10.1016/j.tree.2004.09.004.

Lewison, R.L., Crowder, L.B., Wallace, B.P., Moore, J.E., Cox, T., Zydelis, R., et al. 2014. Global patterns of marine mammal, seabird, and sea turtle bycatch reveal taxa-specific and cumulative megafauna hotspots. Proc. Natl. Acad. Sci. U.S.A. **111**: 5271–5276. doi:10.1073/pnas.1318960111.

Mateo, I., and Hanselman, D.H. 2014. A comparison of statistical methods to standardize catch-per-unit-effort of the Alaska longline sablefish fishery. Available from https://repository.library.noaa.gov/view/noaa/4633 [accessed Mar 18, 2023].

Michelini, E., Cevenini, L., Mezzanotte, L., Simoni, P., Baraldini, M., De Laude, L., and Roda, A. 2007. One-step triplex-polymerase chain reaction assay for the authentication of yellowfin (*Thunnus albacares*), bigeye (*Thunnus obesus*), and skipjack (*Katsuwonus pelamis*) tuna DNA from fresh, frozen, and canned tuna samples. J. Agric. Food Chem. **55**: 7638–7647. doi:10.1021/jf070902k. PMID: 17711337.

Mitchell, J.D., McLean, D.L., Collin, S.P., and Langlois, T.J. 2018. Shark depredation in commercial and recreational fisheries. Rev. Fish Biol. Fish. **28**: 715–748. doi:10.1007/s11160-018-9528-z.

Morissette, L., Kaschner, K., and Gerber, L.R. 2010. 'Whales eat fish'? Demystifying the myth in the Caribbean marine ecosystem. Fish Fish. **11**: 388–404. doi:10.1111/j.1467-2979.2010.00366.x.

Oleson, E.M., Boggs, C.H., Forney, K.A., Hanson, M.B., Kobayashi, D.R., Taylor, B.L., et al. 2010. Status review of Hawaiian insular false killer whales (Pseudorca crassidens) under the Endangered Species Act. U.S. Dept. of Commerce, NOAA Technical memorandum NOAA-TM-NMFS-PIFSC-22.

Peterson, M.J., and Hanselman, D. 2017. Sablefish mortality associated with whale depredation in Alaska. ICES J. Mar. Sci. **74**: 1382–1394. doi:10.1093/icesjms/fsw239.

Peterson, M.J., Mueter, F., Hanselman, D., Lunsford, C., Matkin, C., and Fearnbach, H. 2013. Killer whale (Orcinus orca) depredation effects on catch rates of six groundfish species: implications for commercial longline fisheries in Alaska. ICES J. Mar. Sci. **70**: 1220–1232. doi:10.1093/icesjms/fst045.

Peterson, M.J., Mueter, F., Criddle, K., and Haynie, A.C. 2014. Killer whale depredation and associated costs to Alaskan sablefish, Pacific halibut and Greenland turbot longliners. PLoS ONE, **9**: e88906. doi:10.1371/journal.pone.0088906. PMID: 24558446.

Poncelet, É., Barbraud, C., and Guinet, C. 2010. Population dynamics of killer whales in Crozet Archipelago, southern Indian Ocean: a mark-recapture study from 1977 to 2002. J. Cetacean Res. Manag. **11**: 41–48. doi:10.47536/jcrm.v11i1.629.

R Core Team. 2018. R: a language and environment for statistical computing. R Foundation for Statistical Computing. Available from https://www.R-project.org/ [accessed Mar 18, 2023].

Sagarese, S.R., Frisk, M.G., Cerrato, R.M., Sosebee, K.A., Musick, J.A., Rago, P.J., and Trenkel, V. 2014. Application of generalized additive models to examine ontogenetic and seasonal distributions of spiny dogfish (Squalus acanthias) in the Northeast (US) shelf large marine ecosystem. Can. J. Fish. Aquat. Sci. **71**: 847–877. doi:10.1139/cjfas-2013-0342.

Secchi, E.R., and Vaske, T. 1998. Killer whale (*Orcinus orca*) sightings and depredation on tuna and swordfish longline catches in southern Brazil. Aquat. Mamm. **24**: 117–122.

Shono, H. 2008. Application of the Tweedie distribution to zero-catch data in CPUE analysis. Fish. Res. **93**: 154–162. doi:10.1016/j.fishres.2008.03.006.

Tascheri, R., Saavedra-Nievas, J.C., and Roa-Ureta, R. 2010. Statistical models to standardize catch rates in the multi-species trawl fishery for Patagonian grenadier (Macruronus magellanicus) off Southern Chile. Fish. Res. **105**: 200–214. doi:10.1016/j.fishres.2010.05.010.

TEC Inc. 2009. Cetacean depredation in the Hawaii longline fishery: interviews of longline vessel owners and captains. Report prepared for National Oceanic and Atmospheric Administration National Marine Fisheries Service, Pacific Islands Regional Office, Honolulu, HI.

Thode, A., Wild, L., Straley, J., Barnes, D., Bayless, A., O'Connell, V., et al. 2016. Using line acceleration to measure false killer whale (*Pseudorca crassidens*) click and whistle source levels during pelagic longline depredation. J. Acoust. Soc. Am. **140**: 3941–3951. doi:10.1121/1.4966625. PMID: 27908079.

Tixier, P., Burch, P., Massiot-Granier, F., Ziegler, P., Welsford, D., Lea, M.-A., et al. 2020a. Assessing the impact of toothed whale depredation on socio-ecosystems and fishery management in wide-ranging subantarctic fisheries. Rev. Fish Biol. Fish. **30**: 203–217. doi:10.1007/s11160-020-09597-w.

Tixier, P., Lea, M.-A., Hindell, M.A., Welsford, D., Mazé, C., Gourguet, S., and Arnould, J.P.Y. 2020b. When large marine predators feed on fisheries catches: global patterns of the depredation conflict and directions for coexistence. Fish Fish. **22**: 31–53.

Towers, J.R., Tixier, P., Ross, K.A., Bennett, J., Arnould, J.P.Y., Pitman, R.L., and Durban, J.W. 2019. Movements and dive behaviour of a toothfish-depredating killer and sperm whale. ICES J. Mar. Sci. **76**: 298–311. doi:10.1093/icesjms/fsy118.

Uchiyama, J.H., and Kazama, T.K. 2003. Updated weight-on-length relationships for pelagic fishes caught in the central North Pacific Ocean and bottomfishes from the northwestern Hawaiian Islands. Available from https://repository.library.noaa.gov/view/noaa/4789 [accessed Mar 18, 2023].

Uchiyama, J.H., and Boggs, C.H. 2006. Length-weight relationships of dolphinfish, Coryphaena hippurus, and wahoo, Acanthocybium solandri: seasonal effects of spawning and possible migration in the central North Pacific. Mar. Fish. Rev. **68**: 19–29.

WCPFC. 2019. Western and Central Pacific Fisheries Commission Tuna Fishery Yearbook 2019.Available from https://www.wcpfc.int/doc/wcpfc-tuna-fishery-yearbook-2019 [accessed Mar 18, 2023].

Wood, S. 2006. Generalized additive models: an introduction with R. Chapman and Hall/CRC Press.

Wood, S. 2007. The mgcv package. Available from https://cran.r-project.org/web/packages/mgcv/mgcv.pdf [accessed Mar 18, 2023].

Wood, S., and Scheipl, F. 2014. gamm4: Generalized additive mixed models using mgcv and lme4.Available from https://cran.r-project.org/web/packages/gamm4/gamm4.pdf [accessed Mar 18, 2023].

Wood, S.N. 2017. Generalized additive models: an introduction with R. 2nd ed, CRC Press.

Woodworth-Jefcoats, P.A., and Wren, J.L.K. 2020. Toward an environmental predictor of tuna recruitment. Fish. Oceanogr. **29**: 436–441. doi:10.1111/fog.12487.

WPRFMC. 2022. Annual Stock Assessment and Fishery Evaluation Report for the Pacific Pelagic Fisheries Fishery Ecosystem Plan 2021. *Edited by* T. Remington, M. Fitchett, A. Ishizaki and J. DeMello. Western Pacific Regional Fishery Management Council, Honolulu.

Zuur, A., Ieno, E.N., Walker, N., Saveliev, A.A., and Smith, G.M. 2009. Mixed effects models and extensions in ecology with R. Springer Science & Business Media.